

# Sequence-resolved free energy profiles of stress-bearing vimentin intermediate filaments

Beatrice Ramm<sup>a,1</sup>, Johannes Stigler<sup>a,1,2</sup>, Michael Hinczewski<sup>b</sup>, D. Thirumalai<sup>b</sup>, Harald Herrmann<sup>c</sup>, Günther Woehlke<sup>a</sup>, and Matthias Rief<sup>a,d,3</sup>

<sup>a</sup>Physik Department E22, Technische Universität München, 85748 Garching, Germany; <sup>b</sup>Institute for Physical Science and Technology, University of Maryland, College Park, MD 20742; <sup>c</sup>Functional Architecture of the Cell, German Cancer Research Center, 69120 Heidelberg, Germany; and <sup>d</sup>Nanosystems Initiative Munich, 80799 Munich, Germany

Edited by James A. Spudich, Stanford University School of Medicine, Stanford, CA, and approved June 19, 2014 (received for review February 19, 2014)

**Intermediate filaments (IFs) are key to the mechanical strength of metazoan cells. Their basic building blocks are dimeric coiled coils mediating hierarchical assembly of the full-length filaments. Here we use single-molecule force spectroscopy by optical tweezers to assess the folding and stability of coil 2B of the model IF protein vimentin. The coiled coil was unzipped from its N and C termini. When pulling from the C terminus, we observed that the coiled coil was resistant to force owing to the high stability of the C-terminal region. Pulling from the N terminus revealed that the N-terminal half is considerably less stable. The mechanical pulling assay is a unique tool to study and control seed formation and structure propagation of the coiled coil. We then used rigorous theory-based deconvolution for a model-free extraction of the energy landscape and local stability profiles. The data obtained from the two distinct pulling directions complement each other and reveal a tripartite stability of the coiled coil: a labile N-terminal half, followed by a medium stability section and a highly stable region at the far C-terminal end. The different stability regions provide important insight into the mechanics of IF assembly.**

protein folding | Brownian dynamics simulation | trigger sequence

Intermediate filaments (IFs) serve as “stress buffers” (1) in metazoan cells. They are critical for mechanical resistance of the cell, cell motility, and shape determination (2, 3). IFs are a heterogeneous group of proteins encoded by 70 different genes in humans (4). Three of these genes code for nuclear proteins, termed lamins, the others for various cytoplasmic proteins, such as keratins, found in epithelia, and vimentin, characteristic of mesenchymal cells. All IFs share the same overall structure: a long central  $\alpha$ -helical rod of conserved design that is flanked by non- $\alpha$ -helical head and tail domains of highly varying size. Two individual rod domains wrap around each other to form the basic building block of IF assembly: a dimeric coiled coil (CC) (2).

The structure of the homodimeric rod domain of vimentin may be subdivided into three  $\alpha$ -helical regions termed coils 1A, 1B, and 2 [formerly coil 2A, linker 2, and coil 2B (5)], which are interspaced with non- $\alpha$ -helical linker regions L1 and L12 (Fig. 1A) (6, 7).

The superhelical structure of a left-handed CC reflects the characteristic heptad repeat pattern with positions denoted as *abc-defg*, in which hydrophobic residues occupy positions *a* and *d* (8, 9).

CC motifs are not limited to IFs but occur in an estimated 5–10% of all translated protein sequences (8). Their structural simplicity and diverse functionality make them an important model system for protein folding. Debate still exists regarding the precise events of folding of CCs, ranging from collision of previously unstructured chains to the preformation of short  $\alpha$ -helical segments (10–12). CCs also have become a target of single-molecule force spectroscopy, allowing the study of sequence-resolved folding. Examples are the mapping of the energy landscape of the CC model system GCN4 (13, 14) and the recent characterization of the assembly of the SNARE proteins (15).

Many CCs assemble into higher-order structures, as in the case of IFs. Here, the CC dimers associate laterally into roughly half-staggered antiparallel tetramers that, depending on ionic strength,

further stack upon each other to build so-called unit-length filaments (ULFs) (2, 16, 17). Longitudinal annealing of these ULFs is believed to be mediated by the interaction of both dimer ends from each individual ULF, namely coil 1A and coil 2B, resulting in an “overlap” of successive CC dimers (2, 18). In the last step, the filaments undergo a radial compaction yielding full-length IFs (2) that exhibit unique mechanical properties (19–22). The structural nature of the overlap of coil 1A and coil 2B is still debated (2, 23–25). The CC dimer ends represent hotspots for disease-related mutations in IF proteins (4, 26), further underscoring their functional importance.

Interestingly, coil 2 exhibits high sequence and absolute length conservation across all IFs (1, 27). Moreover, the large C-terminal fragment of coil 2 of vimentin (coil 2B) harbors two structurally interesting features: a stutter (residues 351–354) and the highly conserved region of 25 residues at the C terminus (residues 380–404) (Fig. 1A, *Inset*) (23). A stutter is an insertion of an additional four amino acids at the end of a heptad, thus interrupting the regular *abcdefg* pattern (9). The stutter position in coil 2 of IFs is absolutely conserved (23).

In this study, we present a deconvolution force spectroscopic approach using a combination of experiment and Brownian dynamics simulation, allowing us to measure the full distance-resolved energy landscape of the C-terminal part of vimentin coil 2. Our results yield important insight into the mechanical and thermodynamic stability of IFs, with important consequences for their assembly.

## Significance

**Intermediate filaments (IFs) are an essential part of the cytoskeleton of metazoan cells, responsible for the cell's shape and motility. To exert their mechanical function, IF dimers undergo a complex assembly into long filaments. The dimer ends are thought to mediate assembly. Mutations in these regions are associated with various diseases. We use single-molecule force spectroscopy by optical tweezers to mechanically open the C-terminal part of the dimer of the IF vimentin. Using deconvolution, a specialized analytic method, we can directly assess the stability of the C-terminal dimer end. Relating this stability to the amino acid sequence and structural features of the dimer, we shed light on the early assembly and mechanical properties of IFs.**

Author contributions: B.R., J.S., H.H., G.W., and M.R. designed research; B.R. and J.S. performed research; M.H., D.T., and H.H. contributed new reagents/analytic tools; B.R. and J.S. analyzed data; and B.R., J.S., D.T., H.H., G.W., and M.R. wrote the paper.

The authors declare no conflict of interest.

This article is a PNAS Direct Submission.

<sup>1</sup>B.R. and J.S. contributed equally to this work.

<sup>2</sup>Present address: Department of Biochemistry and Molecular Biophysics, Columbia University, New York, NY 10032.

<sup>3</sup>To whom correspondence should be addressed. Email: mrief@ph.tum.de.

This article contains supporting information online at [www.pnas.org/lookup/suppl/doi:10.1073/pnas.1403122111/-DCSupplemental](http://www.pnas.org/lookup/suppl/doi:10.1073/pnas.1403122111/-DCSupplemental).

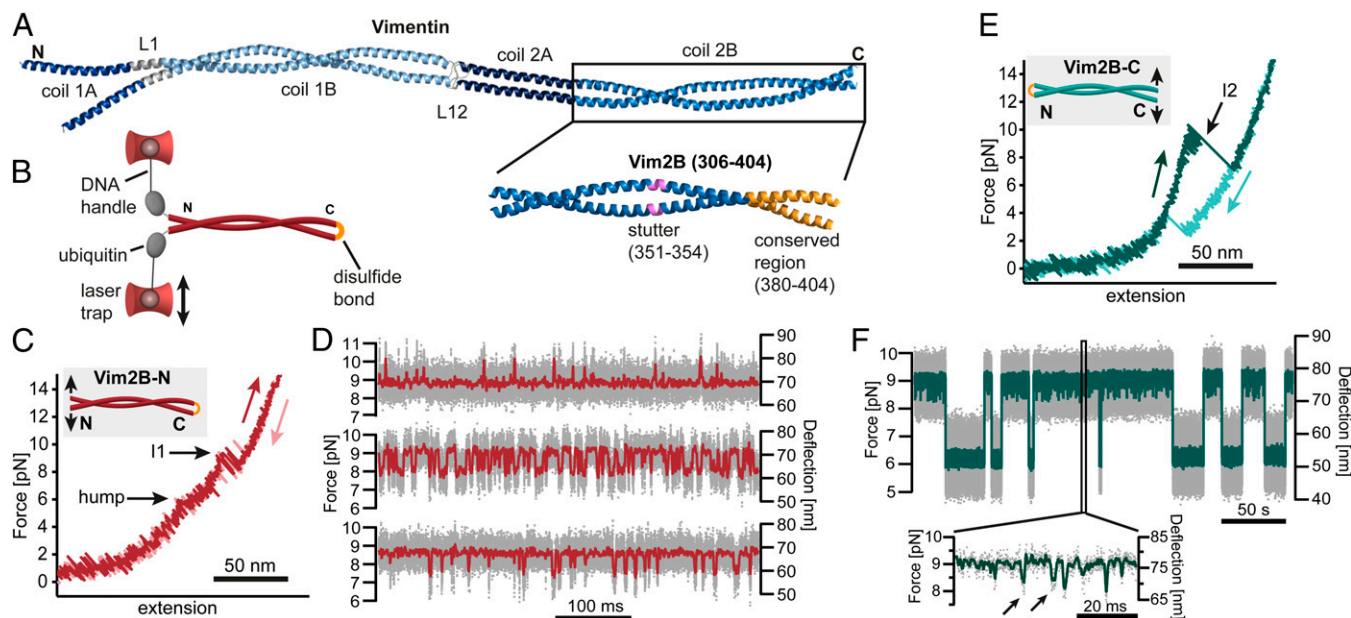


**Fig. 1.** The C-terminal half of coil 2 (Vim2B) shows different folding and unfolding behaviors when unzipped from two different directions. (A) Three-dimensional structural model of a vimentin dimer, save the head and tail domains, provided by A. Chernyatina and S. Strelkov, Laboratory for Biocrystallography, Department of Pharmaceutical and Pharmacological Sciences, Katholieke Universiteit Leuven, Leuven, Belgium (7). (Inset) Structural characteristics of the vimentin coil 2B, in which the stutter is highlighted in purple and the conserved region is marked in orange. (B) Schematic of the experimental setup using the Vim2B-N construct as an example. (C) Representative stretch-and-relax cycle recorded at 500 nm/s for Vim2B-N. Black arrows indicate the two major transitions. (D) Traces recorded in passive mode show equilibrium fluctuations between an intermediate and the unfolded state of Vim2B-N at varying force bias. The CC fluctuates between states mostly residing in the lower unfolded state at higher force bias (Top) and more in the upper partly folded state for decreasing force bias (Middle and Bottom). Full-bandwidth traces (100 kHz) are gray and low-pass filtered traces are colored in red. (E) A representative force-extension trace for Vim2B-C shows a clear three-state behavior (intermediate marked by an arrow). (F) Fluctuations between all three states of the Vim2B-C coil may be monitored in passive mode at a force bias of about 9.1 pN. (Inset) Transition between the folded and intermediate states (intermediate states are marked by an arrow). Full-bandwidth traces (100 kHz) are gray, whereas low-pass filtered traces are colored in green.

## Results

For single-molecule force measurements with the C-terminal half of vimentin coil 2 (Vim2B), we constructed two different fusion proteins containing the vimentin residues 306–404. A terminal cysteine for covalent intradimer linkage and a ubiquitin domain as a spacer for DNA handle attachment were added. By varying the force attachment points, the unfolding pathway of the constructs can be controlled (28–31). One construct (Vim2B-C) was linked by a disulfide bond at the N terminus where mechanical opening proceeds from the C-terminal end. The other construct (Vim2B-N) is opened from the N terminus while linked at the C terminus (Fig. 1B). The unzipping geometry of the linear CCs allows us to assign a precise unfolding coordinate along the backbone of the  $\alpha$ -helices. Using optical tweezers, we performed nonequilibrium experiments recording force-extension traces by stretching and relaxing the constructs at a constant trap velocity of 500 nm/s. Another set of experiments was conducted in “passive mode,” in which the two traps are held at a constant separation, allowing equilibrium fluctuations of the molecule. As we extracted most free energy values and data discussed from passive mode data, hereafter we use the term “stability” synonymously with equilibrium free energy.

### Vimentin Coil 2B Pulled from the N Terminus Unfolds Gradually.

Stretch and relax curves of Vim2B-N are shown in Fig. 1C. Two major transitions close to equilibrium can be observed. Although transitions very close to equilibrium are difficult to observe in force-extension cycles, they appear clearly in an analysis of the force-dependent SD of the signal, in which transition regions appear as areas with increased noise (Fig. S1). Between 5 and 8 pN, we observe a hump-like transition in which the CC gradually unfolds to a metastable intermediate (I1). In the second transition, at forces between 8.5 and 10 pN, the coil

rapidly fluctuates between I1 and the unfolded state. The average contour length increase of  $35.4 (\pm 2.0)$  nm for the first transition indicates that the N-terminal half of coil 2B is already unfolded at around 8 pN. The contour length increase of  $65.4 (\pm 2.3)$  nm between the completely folded and unfolded states corresponds to the unfolding of  $90 (\pm 3)$  residues, indicating that the first 8 N-terminal residues are likely to be unfolded at our minimally resolvable forces of about 2–3 pN. The close-to-equilibrium nature of the first hump-like transition allows us to analyze the cooperativity of the transition and infer the number of intermediates populated (SI Appendix, section 4.2 and Fig. S2). We find that the hump-like transition involves at least one additional intermediate that exchanges quickly with the folded state and the intermediate I1. Because rapid transitions reflect low transition barriers, we infer that the energy landscape of Vim2B-N is flat at its N terminus. Fig. 1D shows passive mode recordings of force-dependent equilibrium fluctuations between I1 and the unfolded state. Increasing force gradually shifts the probability distribution toward the unfolded state (bottom to top traces). Force-dependent state occupancies allow extraction of equilibrium free energy differences (SI Appendix, section 4.4). The free energy difference between the unfolded state and I1 is  $22.3 k_B T$ , roughly reflecting the stability of the C-terminal half of Vim2B-N. The folding free energy of the whole construct is  $35.2 (\pm 3.5) k_B T$ , as obtained by integrating the force-extension trace across the complete transition (SI Appendix, section 4.4). Hence, two thirds of the total free energy is provided by the C-terminal half.

### Vimentin Coil 2B Unfolds in a Clear Three-State Manner When Pulled from the C Terminus.

The unfolding/folding pattern of Vim2B-C seemingly is very different from that of Vim2B-N. The stretch-and-relax cycles show a steep rise up to 8 pN, corresponding to the stretching of the DNA handles. Between 8 and 10 pN, the

protein fluctuates quickly between the folded state and an obligatory intermediate (I2) (Fig. 1E). The contour length increase associated with unfolding into I2 is about  $14.2 (\pm 2.0)$  nm ( $19 \pm 3$  amino acids) and corresponds to the unfolding of nearly all residues of the conserved C-terminal region of coil 2B. At about 10 pN, the rest of the CC rips in one step to the fully unfolded state. The overall contour length increase of  $69.5 (\pm 2.0)$  nm corresponds to  $95 (\pm 3)$  folded amino acids and is close to the expected value for a fully folded CC (98 residues). Unfolding and refolding traces display a pronounced hysteresis, with refolding occurring only if the force is lowered below 5 pN at a trap velocity of 500 nm/s. This hysteresis demonstrates that Vim2B-C is much further from equilibrium than Vim2B-N. Nevertheless, we could observe slow folding/unfolding transitions of Vim2B-C between the fully folded state and the unfolded state (Fig. 1F) in passive mode. In addition to the slow folding/unfolding kinetics, rapid population of I2 from the folded state may be observed (Fig. 1F, *Inset*). Analysis of the equilibrium population under force yields a total free energy of  $36.8 (\pm 3.7) k_B T$  for Vim2B-C,  $12.9 (\pm 1.3) k_B T$  of which is contributed by the last 19 C-terminal residues unfolded in the intermediate. Hence, these 19 amino acids contribute about one third of the total free energy while comprising only one fifth of the total number of residues. We find the overall free energy is similar to the one obtained from the Vim2B-N construct. All lengths and energies of Vim2B-N and Vim2B-C are summarized in Table S1.

**Deconvolution Allows a More Elaborate Insight into the Energy Landscape of the Constructs.** To obtain a more detailed view of the energy landscape of coil 2B, we used deconvolution force spectroscopy (13, 32). In brief, in an optical tweezers experiment, the fluctuations of the ends of the CC are blurred by the thermal movements of beads attached to the DNA handles (Fig. 2A, gray line). Hence, bead position is not a faithful reporter of the actual protein extension, because the beads can move by extending the DNA, even if the protein ends do not. Given good knowledge of the thermal fluctuations of beads and handles, we can remove this blur from the passive mode data (Fig. 1D and F) by deconvolution and recover the intrinsic probability distribution of the fluctuations, owing to the opening of the CC (Fig. 2A, solid red and green lines; for details, see *Methods* and *SI Appendix*).

Using the Boltzmann equilibrium (Eq. S8), we can compute the energy landscapes of the CCs directly from the deconvolved probability distributions (Fig. 2B, solid lines). A comparison with the energy landscapes obtained from distributions before deconvolution (Fig. 2B, dotted lines) demonstrates the gain in fine structure upon deconvolution. Back transformation of the energy landscapes measured under force yielded the energy landscapes of Vim2B-N and Vim2B-C when no load is applied (Fig. 2C) (*SI Appendix*, section 5.3). The values obtained by the “conventional” energetic analysis (points in Fig. 2C) fit neatly onto the energy landscapes, validating the deconvolution procedure.

For additional validation of the inferred energy landscapes, we performed simulations of stretch-relax cycles for Vim2B-C and Vim2B-N based on the deconvolved energy landscapes of Fig. 2C. To this end, we modeled the contour length change of the protein as a diffusive process in the corresponding energy landscape. This process was coupled via worm-like chain linkers to beads that were allowed to diffuse in harmonic trap potentials. While gradually increasing/decreasing the trap distance, we simulated the equation of motion of the beads and the trajectory of the end-to-end distance of the protein. The bead trajectories then were converted directly to force-extension traces. For further details of the simulations, see *Methods* and *SI Appendix*. The result of stretch-and-relax cycle simulations performed at 500 nm/s pulling velocity for Vim2B-N and Vim2B-C is shown in *SI Appendix*, Fig. S3. For both constructs, the force-extension profiles of these cycles agree well with measured traces (compare to Fig. 1C and E). The simulations reproduce all basic features, such as intermediate states and the gradual unfolding of the N

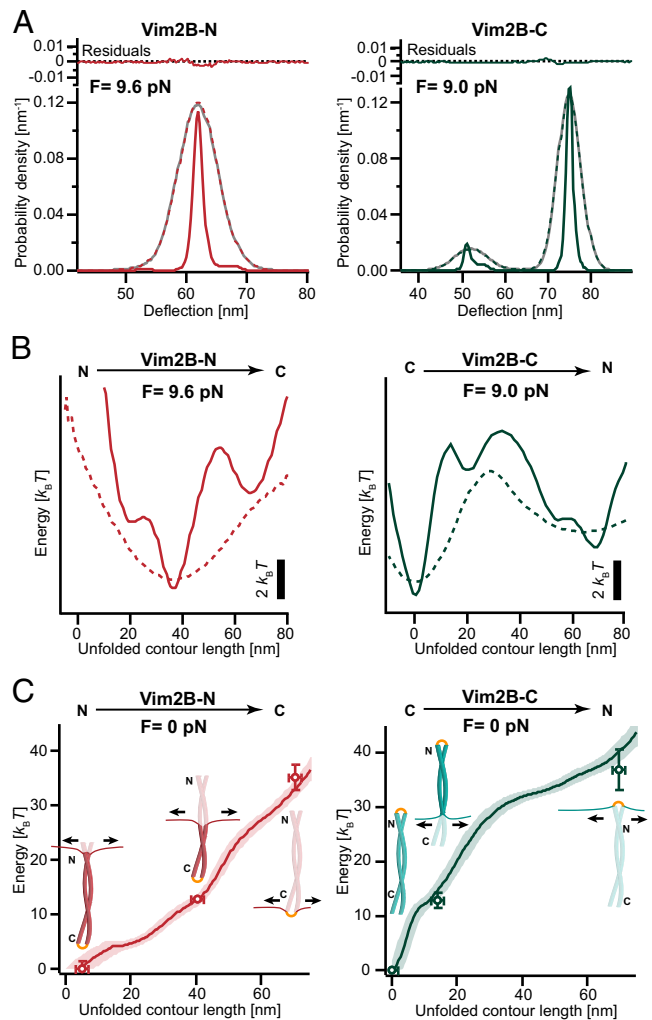


**Fig. 2.** Model-free reconstruction of the full energy landscapes of Vim2B-N and Vim2B-C obtained by deconvolution. (A) The protein probability distributions of Vim2B-N (red, *Left*) and Vim2B-C (green, *Right*) may be obtained from the bead deflection probability distributions (gray) by deconvolution. The residuals show the difference between the reconvoled form of the deconvolved probability distributions (colored, dotted lines) and the measured distributions (gray line). (B) The deconvolved energy landscapes of Vim2B-N (continuous red line, *Left*) and Vim2B-C (continuous green line, *Right*) under force provide more details than the original bead position-derived landscapes (dotted lines). (C) Energy landscapes of Vim2B-N (red, *Left*) and Vim2B-C (green, *Right*) in the absence of force. Shaded areas are 68% confidence intervals obtained by bootstrapping. Points are values obtained from conventional data analysis (*SI Appendix*, section 4.4 and Table S1).

terminus of Vim2B-N, as well as the hysteresis in Vim2B-C, proving the validity of the deconvolved landscapes.

To be able to compare the two energy landscapes obtained by unzipping Vim2B from two different ends, we calculated the differential energy profiles (i.e.,  $dG/dL$ ) for both constructs (*SI Appendix*, section 5.8). These local stability profiles of the CC are shown in Fig. 3, with the length coordinate corresponding to Vim2B-N. Note that in this representation, the profile of Vim2B-C is reversed compared with its energy landscape in Fig. 2C. This local stability can be matched with its primary sequence. To simplify the sequence, only the *a*- and *d*-positions that form the hydrophobic seam are displayed in Fig. 3. Although the two energy profiles agree very well within errors in a large part along the sequence, there are notable differences, which we discuss below.

We find that the CC can be divided roughly into a labile N-terminal half (region I) with stability not exceeding  $0.5 k_B T/nm$  and a stable C-terminal part. In Vim2B-C (green), protein stability at the C terminus is unaffected by contributions from seed formation (*Discussion*). In this construct, the C-terminal region may be subdivided further into two sections (II and III) that are separated by a local stability minimum. The upstream section (region II) displays intermediate stability, whereas the downstream section (region III) is very stable, with values increasing to nearly  $2 k_B T/nm$ .

## Discussion

**Entropic Cost for Seed Formation and Exchanged Sites of Cross-Linking Account for the Differences in the Differential Energy Profiles.** In general, different pulling directions sample different reaction coordinates in a protein's energy landscape (28–31). However, in our experiments, the measured unfolding free energy profiles of Vim2B-N and Vim2B-C reflect the piecewise opening of the CC contacts, starting in a folded conformation and ending in a stretched and fully unfolded conformation. Even though the sequence of opening is reversed for both constructs, one would expect the free energy profiles to proceed along a similar reaction coordinate, albeit with reversed orientation, and hence contain very similar information. However, when looking at the force-extension traces (Fig. 1 *C* and *E*), one notices different intermediates I1 and I2 in the unfolding of Vim2B-N and Vim2B-C.

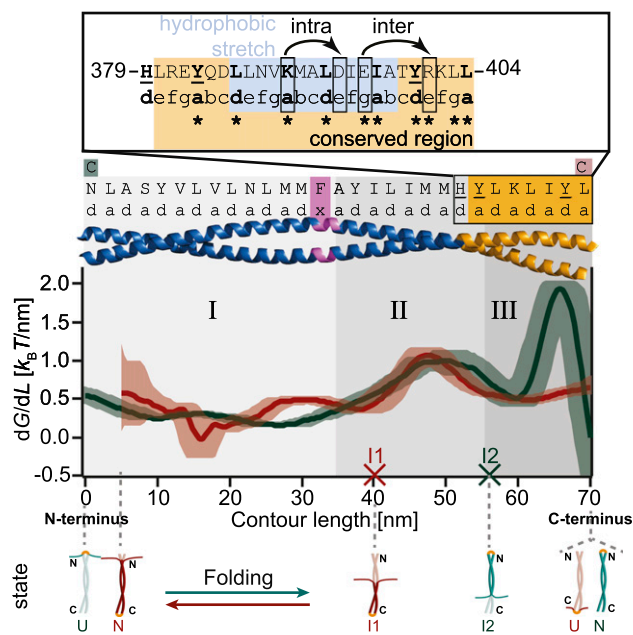


**Fig. 3.** The energy profiles of Vim2B-N (red) and Vim2B-C (green) reveal a tripartite stability of the CC. Derivative of the energy landscapes of Vim2B-N (red) and Vim2B-C (green) with respect to contour length aligned at the C-terminal end. The derivatives of the energy landscape describe the energy needed to unfold a certain part of the CC and therefore may be interpreted as a local stability profile (*SI Appendix*). The contour lengths of the intermediates I1 and I2 obtained by conventional data analysis are indicated by red and green crosses. Shaded areas are 68% confidence intervals from bootstrapping. The first 5 nm of the stability profile of Vim2B-N are not shown, as errors exceed 100%. The residues occupying *a*- and *d*-positions of the CC are listed on top. Cysteine mutations are colored red/green according to construct. (*Inset*) Features of the conserved region (orange). The position of the stutter is marked in purple. The main hydrophobic stretch of coil 2B is highlighted in blue. Bulky residues causing local stability minima are underlined. Bent arrows indicate the intra- and interhelical salt bridges. Asterisks mark absolutely conserved residues that are unchanged in seven human IF proteins constituting major representatives of all five sequence homology classes of IFs (23).

In addition, the discrepancy between the pronounced hysteresis of Vim2B-C and the close-to-equilibrium fluctuations of Vim2B-N (Fig. 1 *C* and *E*) recorded at identical pulling speeds is striking. Moreover, the energy profiles derived from Vim2B-N and Vim2B-C seem to diverge, especially at the C-terminal end (Fig. 3).

These discrepancies may be explained by two different contributions: First, the need for cross-linking cysteines makes the two protein sequences slightly different. Second, nucleation seed formation that starts folding will occur at different termini in the two constructs. Hence, the free energy profile of Fig. 3 also contains the entropic cost of ordering the residues forming the nucleation seed for further propagation. We argue that the asymmetry caused by the exchanged sites of cross-linking and force application is a major determinant of the observed differences.

Ensemble studies have shown that folding of a CC is initiated by a nucleation mechanism that involves the collision of unstructured or preformed  $\alpha$ -helical chains forming a CC (10, 12, 33). The different cross-linking geometries used in our mechanical unzipping assays allow us to control at which terminus of the protein this nucleation seed forms. According to Sosnick and coworkers (11), introducing a cross-link between the two chains of a CC forces the CC to nucleate at the cross-linked end. Under mechanical load, seed formation at the distal end is inhibited further by the energy costs associated with bringing the untethered ends together. Hence, folding of Vim2B-C demands seed formation at the labile N terminus, whereas the formation of the Vim2B-N coil involves seed formation at the stable C terminus (region III).

The effect of seed formation is clearly visible in region III (Fig. 3) at the C terminus, where the green curve (Vim2B-C) lies above the red curve (Vim2B-N), as the Vim2B-N construct has to form its seed at the C terminus whereas Vim2B-C has already adopted the CC structure at this position. Thus, Vim2B-N consumes the free energy provided by the favorable interactions of the two chains to form the seed, whereas Vim2B-C does not. As the entropic cost paid for seed formation should be similar for both constructs, a comparable discrepancy between the two traces also should occur at the N-terminal end, where Vim2B-C has to pay the price for seed formation instead of Vim2B-N. However, at the N terminus, the red trace seems to lie only marginally above the green trace. At this point, it is important to note that the cross-links introduce a divergence at the sequence level among the two constructs. Vim2B-C is cross-linked at the N terminus where the cysteine replaces an asparagine. In contrast, Vim2B-N is cross-linked at the C terminus, with the cysteine replacing a leucine. Stability studies of CCs have shown that introducing an asparagine at a *d*-position is energetically unfavorable and destabilizes a CC by  $1.0 k_B T$ , whereas leucine at the *a*-position stabilizes by  $5.9 k_B T$  compared with a CC with an alanine in the same position (34–36). Hence, the measured free energy profile of Vim2B-C overestimates the free energy at the N terminus compared with the profile of Vim2B-N. Similarly, the profile of Vim2B-N underestimates the free energy at the C terminus relative to Vim2B-C, because it misses the last favorable leucine contact substituted by a nonopening cysteine cross-link. To illustrate those effects, we show a modified energy profile in Fig. S4, in which we try to restore the energetic equality between the two constructs.

After this correction, the free energies for seed formation (hatched areas in Fig. S4) may be estimated to be about  $4 k_B T$ . Even though direct information about seed length is missing, in this representation, the seed of Vim2B-C is longer, whereas we assume the seed of Vim2B-N is more localized owing to the high stability of region III at the C terminus.

It has been proposed that the highly stable C-terminal end of the CC (region III) harbors a trigger sequence (37) offering a site for seed formation in the initial stage of folding. Trigger sequences have been reported for many CCs; however, whether they are indispensable for folding is debated (38–41). It appears that a main role of trigger sequences is to offer enough free energy (13, 42) to overcome the cost of seed formation, which is



shape of noise, the impact of force on the end-to-end distance of the protein (i.e., the force-dependent folding/unfolding trajectories), and the coupling of the responses of protein and beads. To this end, we concurrently simulated the coupled time evolution of the coordinates  $x$  and  $L_p$  in the potential  $\mathcal{H}_d(x, L_p)$  using Langevin dynamics. These simulations describe the noise of the thermal fluctuations in the trap as well as the coupled dynamics of the end-to-end distance of the protein:

$$\begin{aligned}\Delta x &= \frac{\Delta t}{\gamma_b} \left( -\frac{\partial \mathcal{H}_d}{\partial x}(x, L_p) k_B T + \sqrt{2k_B T \frac{\gamma_b}{\Delta t}} \varepsilon(t) \right), \\ \Delta L_p &= \frac{\Delta t}{\gamma_p} \left( -\frac{\partial \mathcal{H}_d}{\partial L_p}(x, L_p) k_B T + \sqrt{2k_B T \frac{\gamma_p}{\Delta t}} \varepsilon(t) \right),\end{aligned}$$

where  $\varepsilon(t)$  describes white noise with an SD of  $\sigma = 1$ . The friction coefficient  $\gamma_b$  is dominated by hydrodynamic friction on the beads and was calculated

- Herrmann H, Aebi U (2004) Intermediate filaments: Molecular structure, assembly mechanism, and integration into functionally distinct intracellular scaffolds. *Annu Rev Biochem* 73(1):749–789.
- Herrmann H, Strelkov SV, Burkhard P, Aebi U (2009) Intermediate filaments: Primary determinants of cell architecture and plasticity. *J Clin Invest* 119(7):1772–1783.
- Goldman RD, Cleland MM, Murthy SN, Mahammad S, Kuczumarski ER (2012) Inroads into the structure and function of intermediate filament networks. *J Struct Biol* 177(1):14–23.
- Szeverenyi I, et al. (2008) The Human Intermediate Filament Database: Comprehensive information on a gene family involved in many human diseases. *Hum Mutat* 29(3):351–360.
- Steinert PM, Marekov LN, Parry DA (1993) Diversity of intermediate filament structure. Evidence that the alignment of coiled-coil molecules in vimentin is different from that in keratin intermediate filaments. *J Biol Chem* 268(33):24916–24925.
- Chernyatina AA, Strelkov SV (2012) Stabilization of vimentin coil2 fragment via an engineered disulfide. *J Struct Biol* 177(1):46–53.
- Chernyatina AA, Nicolet S, Aebi U, Herrmann H, Strelkov SV (2012) Atomic structure of the vimentin central  $\alpha$ -helical domain and its implications for intermediate filament assembly. *Proc Natl Acad Sci USA* 109(34):13620–13625.
- Moutevelis E, Woolfson DN (2009) A periodic table of coiled-coil protein structures. *J Mol Biol* 385(3):726–732.
- Lupas AN, Gruber M (2005) The structure of alpha-helical coiled coils. *Adv Protein Chem* 70:37–78.
- Zitzewitz JA, Ibarra-Molero B, Fishel DR, Terry KL, Matthews CR (2000) Preformed secondary structure drives the association reaction of GCN4-p1, a model coiled-coil system. *J Mol Biol* 296(4):1105–1116.
- Moran LB, Schneider JP, Kentis A, Reddy GA, Sosnick TR (1999) Transition state heterogeneity in GCN4 coiled coil folding studied by using multisite mutations and crosslinking. *Proc Natl Acad Sci USA* 96(19):10699–10704.
- Meisner WK, Sosnick TR (2004) Fast folding of a helical protein initiated by the collision of unstructured chains. *Proc Natl Acad Sci USA* 101(37):13478–13482.
- Gebhardt JC, Bornschlöggl T, Rief M (2010) Full distance-resolved folding energy landscape of one single protein molecule. *Proc Natl Acad Sci USA* 107(5):2013–2018.
- Gao Y, Sirinakis G, Zhang Y (2011) Highly anisotropic stability and folding kinetics of a single coiled coil protein under mechanical tension. *J Am Chem Soc* 133(32):12749–12757.
- Gao Y, et al. (2012) Single reconstituted neuronal SNARE complexes zipper in three distinct stages. *Science* 337(6100):1340–1343.
- Sokolova AV, et al. (2006) Monitoring intermediate filament assembly by small-angle x-ray scattering reveals the molecular architecture of assembly intermediates. *Proc Natl Acad Sci USA* 103(44):16206–16211.
- Mücke N, et al. (2004) Molecular and biophysical characterization of assembly-starter units of human vimentin. *J Mol Biol* 340(1):97–114.
- Smith TA, Strelkov SV, Burkhard P, Aebi U, Parry DAD (2002) Sequence comparisons of intermediate filament chains: Evidence of a unique functional/structural role for coiled-coil segment 1A and linker L1. *J Struct Biol* 137(1–2):128–145.
- Mücke N, et al. (2004) Assessing the flexibility of intermediate filaments by atomic force microscopy. *J Mol Biol* 335(5):1241–1250.
- Staple DB, Loparic M, Kreuzer HJ, Kreplak L (2009) Stretching, unfolding, and deforming protein filaments adsorbed at solid-liquid interfaces using the tip of an atomic-force microscope. *Phys Rev Lett* 102(12):128302.
- Kreplak L, Fudge D (2007) Biomechanical properties of intermediate filaments: From tissues to single filaments and back. *BioEssays* 29(1):26–35.
- Swift J, et al. (2013) Nuclear lamin-A scales with tissue stiffness and enhances matrix-directed differentiation. *Science* 341(6149):1240104.
- Strelkov SV, et al. (2002) Conserved segments 1A and 2B of the intermediate filament dimer: Their atomic structures and role in filament assembly. *EMBO J* 21(6):1255–1266.
- Kapinos LE, et al. (2010) Characterization of the head-to-tail overlap complexes formed by human lamin A, B1 and B2 “half-minilamin” dimers. *J Mol Biol* 396(3):719–731.
- Strelkov SV, Schumacher J, Burkhard P, Aebi U, Herrmann H (2004) Crystal structure of the human lamin A coil 2B dimer: Implications for the head-to-tail association of nuclear lamins. *J Mol Biol* 343(4):1067–1080.

from first principles, whereas the friction coefficient of movement in the protein energy landscape  $\gamma_p$  was matched against measured transition rates. The mechanical parameters were chosen to mimic experimental conditions. Simulations were performed at time steps of  $10^{-7}$  s and sampled at 20 kHz while the trap distance  $d$  was varied continuously. Stretch-relax cycles then were obtained from the bead deflection trajectory  $x(t)$ . *SI Appendix* contains a detailed description.

**ACKNOWLEDGMENTS.** We thank Anastasia A. Chernyatina and Sergei V. Strelkov for providing the three-dimensional structural model of the vimentin dimer. J.S. was supported by the Elitenetzwerk Bayern in the framework of the doctorate program Material Science of Complex Interfaces. D.T. is grateful to the National Institutes of Health for partial support through Grant GM 089685. M.R. acknowledges support through a Sonderforschungsbereich 863 A2 grant from Deutsche Forschungsgemeinschaft.

- Clemen CS, Herrmann H, Strelkov SV, Schröder R (2013) Desminopathies: Pathology and mechanisms. *Acta Neuropathol* 125(1):47–75.
- Parry DAD, Steinert PM (1999) Intermediate filaments: Molecular architecture, assembly, dynamics and polymorphism. *Q Rev Biophys* 32(2):99–187.
- Dietz H, Rief M (2006) Protein structure by mechanical triangulation. *Proc Natl Acad Sci USA* 103(5):1244–1247.
- Brockwell DJ, et al. (2003) Pulling geometry defines the mechanical resistance of a beta-sheet protein. *Nat Struct Biol* 10(9):731–737.
- Shank EA, Ceccoli C, Dill JW, Marqusee S, Bustamante C (2010) The folding cooperativity of a protein is controlled by its chain topology. *Nature* 465(7298):637–640.
- Carrion-Vazquez M, et al. (2003) The mechanical stability of ubiquitin is linkage dependent. *Nat Struct Biol* 10(9):738–743.
- Woodside MT, et al. (2006) Direct measurement of the full, sequence-dependent folding landscape of a nucleic acid. *Science* 314(5801):1001–1004.
- Bornschlöggl T, Gebhardt JCM, Rief M (2009) Designing the folding mechanics of coiled coils. *ChemPhysChem* 10(16):2800–2804.
- Bornschlöggl T, Rief M (2006) Single molecule unzipping of coiled coils: Sequence resolved stability profiles. *Phys Rev Lett* 96(11):118102.
- Tripet B, Wagschal K, Lavigne P, Mant CT, Hodges RS (2000) Effects of side-chain characteristics on stability and oligomerization state of a de novo-designed model coiled-coil: 20 amino acid substitutions in position “d.” *J Mol Biol* 300(2):377–402.
- Wagschal K, Tripet B, Lavigne P, Mant C, Hodges RS (1999) The role of position a in determining the stability and oligomerization state of  $\alpha$ -helical coiled coils: 20 amino acid stability coefficients in the hydrophobic core of proteins. *Protein Sci* 8(11):2312–2329.
- Wu KC, et al. (2000) Coiled-coil trigger motifs in the 1B and 2B rod domain segments are required for the stability of keratin intermediate filaments. *Mol Biol Cell* 11(10):3539–3558.
- Steinmetz MO, et al. (2007) Molecular basis of coiled-coil formation. *Proc Natl Acad Sci USA* 104(17):7062–7067.
- Kammerer RA, et al. (1998) An autonomous folding unit mediates the assembly of two-stranded coiled coils. *Proc Natl Acad Sci USA* 95(23):13419–13424.
- Burkhard P, Kammerer RA, Steinmetz MO, Bourenkov GP, Aebi U (2000) The coiled-coil trigger site of the rod domain of cortexillin I unveils a distinct network of interhelical and intrahelical salt bridges. *Structure* 8(3):223–230.
- Lee DL, Lavigne P, Hodges RS (2001) Are trigger sequences essential in the folding of two-stranded  $\alpha$ -helical coiled-coils? *J Mol Biol* 306(3):539–553.
- Ibarra-Molero B, Zitzewitz JA, Matthews CR (2004) Salt-bridges can stabilize but do not accelerate the folding of the homodimeric coiled-coil peptide GCN4-p1. *J Mol Biol* 336(5):989–996.
- Matthews CR (1987) Effect of point mutations of the folding of globular proteins. *Methods Enzymol* 154:498–511.
- Fersht AR, Matouschek A, Serrano L (1992) The folding of an enzyme. I. Theory of protein engineering analysis of stability and pathway of protein folding. *J Mol Biol* 224(3):771–782.
- Herrmann H, et al. (2000) The intermediate filament protein consensus motif of helix 2B: Its atomic structure and contribution to assembly. *J Mol Biol* 298(5):817–832.
- Goudeau B, et al. (2006) Variable pathogenic potentials of mutations located in the desmin alpha-helical domain. *Hum Mutat* 27(9):906–913.
- Bär H, et al. (2005) Severe muscle disease-causing desmin mutations interfere with in vitro filament assembly at distinct stages. *Proc Natl Acad Sci USA* 102(42):15099–15104.
- Bär H, et al. (2006) Impact of disease mutations on the desmin filament assembly process. *J Mol Biol* 360(5):1031–1042.
- Meier M, et al. (2009) Vimentin coil 1A-A molecular switch involved in the initiation of filament elongation. *J Mol Biol* 390(2):245–261.
- Stigler J, Rief M (2012) Hidden Markov analysis of trajectories in single-molecule experiments and the effects of missed events. *ChemPhysChem* 13(4):1079–1086.
- Hinczewski M, Gebhardt JCM, Rief M, Thirumalai D (2013) From mechanical folding trajectories to intrinsic energy landscapes of biopolymers. *Proc Natl Acad Sci USA* 110(12):4500–4505.